ORIGINAL ARTICLE

Glucose metabolic profiles evaluated by PET associated with molecular characteristic landscape of gastric cancer

Seong-Woo Bae[1] · Felix Berlth[2] · Kyoung-Yun Jeong[1] · Ji-Hyeon Park[3] · Jong-Ho Choi[3] · Shin-Hoo Park[3] ·
Yun-Suhk Suh[3] · Seong-Ho Kong[3] · Do-Joong Park[3] · Hyuk-Joon Lee[1,3] · Charles Lee[5] · Jong-Il Kim[1,6] ·
Hyewon Youn[1,4] · Hongyoon Choi[4] · Gi Jeong Cheon[1,4] · Keon Wook Kang[1,4] · Han-Kwang Yang[1,3]

Abstract

Background Although FDG-PET is widely used in cancer, its role in gastric cancer (GC) is still controversial due to variable [^{18}F]fluorodeoxyglucose ([^{18}F]FDG) uptake. Here, we sought to develop a genetic signature to predict high FDG-avid GC to plan individualized PET and investigate the molecular landscape of GC and its association with glucose metabolic profiles noninvasively evaluated by [^{18}F]FDG-PET.

Methods Based on a genetic signature, PETscore, representing [^{18}F]FDG avidity, was developed by imaging data acquired from thirty patient-derived xenografts (PDX). The PETscore was validated by [^{18}F]FDG-PET data and gene expression data of human GC. The PETscore was associated with genomic and transcriptomic profiles of GC using The Cancer Genome Atlas.

Results Five genes, *PLS1, PYY, HBQ1, SLC6A5, and NAT16*, were identified for the predictive model for [^{18}F]FDG uptake of GC. The PETscore was validated in independent PET data of human GC with qRT-PCR and RNA-sequencing. By applying PETscore on TCGA, a significant association between glucose uptake and tumor mutational burden as well as genomic alterations were identified.

Conclusion Our findings suggest that molecular characteristics are underlying the diverse metabolic profiles of GC. Diverse glucose metabolic profiles may apply to precise diagnostic and therapeutic approaches for GC.

Seong-Woo Bae and Felix Berlth contributed equally.

✉ Hongyoon Choi
hkyang@snu.ac.kr; chy1000@snu.ac.kr

✉ Han-Kwang Yang
hkyang@snu.ac.kr; chy1000@snu.ac.kr

[1] Cancer Research Institute, Seoul National University College of Medicine, Seoul, Republic of Korea

[2] Department of General, Visceral and Transplant Surgery, University of Mainz, Mainz, Germany

[3] Department of Surgery, Seoul National University Hospital, 101 Daehak-ro, Jongno-gu, Seoul 03080, Republic of Korea

[4] Department of Nuclear Medicine, Seoul National University Hospital, 101 Daehak-ro, Jongno-gu, Seoul 03080, Republic of Korea

[5] The Jackson Laboratory for Genomic Medicine, Farmington, CT, USA

[6] Department of Biomedical Sciences, Seoul National University College of Medicine, Seoul, Republic of Korea

Introduction

Gastric cancer (GC) is characterized by its tumor heterogeneity at molecular, histological, and phenotypic levels [1]. Precise molecular characterization as well as an accurate diagnosis is essential for the management of GC. For tumor staging, various medical imaging modalities including computerized tomography (CT), Magnetic Resonance Imaging (MRI), endoscopic ultrasound imaging (EUS), and positron emission tomography (PET), are commonly used [2]. Unlike other imaging modalities, 2-Deoxy-2-[^{18}F]fluoro-D-glucose ([^{18}F]FDG) PET has been established as a noninvasive tool for evaluating glucose metabolism of tumor based on the principle of high rate of glucose consumption in cancers [3]. However, the clinical utility of [^{18}F]FDG-PET in gastric cancer remains controversial because of the diversity in metabolic profiles of GC [4]. The detection rate of [^{18}F]FDG-PET scan in GC lesion is less than 50% for early gastric cancers (EGC) and 62–98% for advanced gastric cancers (AGC) [5,

6]. Furthermore, prospective trials failed to predict treatment response on gastric cancer by its [18F]FDG-PET scan results [7]. One of the reasons for diagnostic inaccuracy is the presence of low [18F]FDG-avid GC expressing the well-known heterogeneity of this tumor entity. Low FDG-avid GC includes the diffuse type GC and signet ring cell type with high mucinous content and lower cellularity [8–10]. In other words, as GC includes various subtypes according to histology as well as underlying genomic alterations, heterogeneous metabolic profiles correspond to a broad range of [18F]FDG avidity. Nonetheless, genomic and transcriptomic features associated with the variable glucose metabolic profiles have not yet been fully investigated. Understanding the glucose metabolic characteristics of GC is therefore of paramount importance to apply a rational selection on GC subtypes for [18F]FDG-PET scan.

Here, we comprehensively interrogate the association between molecular landscape and glucose metabolic profiles non-invasively evaluated by PET of human gastric cancer patient-derived xenograft (PDX) models as well as human GC. It aims to understand the underlying molecular features associated with [18F]FDG-PET imaging. Functional gene expression networks related to FDG avidity were identified and applied to develop a gene signature, PETscore. PETscore predicted FDG avidity of GC and was validated in independent datasets. Furthermore, we investigated genomic alterations and metabolic profiles associated with PETscore using The Cancer Genome Atlas (TCGA) data.

Materials and methods

Establishment of human gastric cancer PDX

Gastric cancer (GC) tissues were obtained from patients who underwent gastrectomies at Seoul National University Hospital in 2014 and 2017 with informed consent, and the study was approved by the institutional review board (IRB) of Seoul National University Hospital (No. 1402-054-555) in accordance with the Declaration of Helsinki. Establishing GC PDXs was conducted in collaboration with the Jackson Laboratory and mice cared for according to institutional guidelines of the Institutional Animal Care and Use Committee of the Seoul National University (No. 14-0016-C0A0). Immediately after the tissue acquisition, the human tissue samples were transferred to RPMI 1640 medium with 1% penicillin/streptomycin (all from Thermo Fisher Scientific, Waltham, MA, USA). The human tumor tissues were minced into pieces approximately 2 mm in size and subcutaneously injected into the flanks of 6-week-old female NOD. Cg-Prkdc^scid Il2rg^tm1Wjl/SzJ(NSG™) mice (The Jackson Laboratory, Bar Harbor, ME, USA). The tumor volume and bodyweight of the mice were checked once or twice weekly. The

volume was calculated as $(\text{length} \times \text{width}^2)/2$. When tumor volumes reached > 700 to 1000 mm³, mice were euthanized, and tumor tissues were excised and cryopreserved in liquid nitrogen to generate next passage PDXs. Each successful PDX line was assigned a unique ID (SNU-JAX-GXXX). Thirty cases among the established PDXs were available for the present study. The clinical characteristics of the PDX samples are summarized in Table 1.

Human [18F]FDG PET imaging and analysis

PET imaging of patients was collected. According to the standard protocol of our hospital, patients were injected intravenously 5.18 MBq/kg of FDG after fasting for at least 6 h with blood glucose level < 140 mg/kg. PET/CT scans were started 60 min after injection, using dedicated PET/CT scanners or a PET/MR scanner (Biograph 40, mCT, and mMR, Siemens). An emission scan was acquired from the skull base to the proximal thigh. A CT scan was also obtained for attenuation correction. For PET/MR, attenuation correction map was generated by DIXON sequence. PET images were reconstructed using an iterative algorithm (ordered-subset expectation maximization). All PET images were reviewed by the experienced nuclear medicine physician using commercial imaging software (Syngo.via, VA 30; Siemens Healthcare, Erlangen, Germany). To evaluate FDG uptake of tumors, spherical volume of interests (VOIs) was drawn for each patient. In each VOI, the maximum standardized uptake value (SUVmax) was measured.

Small animal [18F]FDG PET imaging and analysis

Six-week-old female BALB/c nu/nu mice (Orient Bio., Sungnam, Korea) were used to establish PDX tumor mouse models ($n = 3$ per PDX case). The mouse tumor modeling,

Table 1 Characteristics of human gastric cancer PDX tissues

Variable	n (%)
Total no. of PDX cases	30
Lauren classification	
Intestinal	10 (33.3%)
Diffuse	9 (30%)
Mixed	9 (30%)
Undetermined	2 (6.7%)
WHO classification	
Well differentiated tubular adenocarcinoma	1 (3.3%)
Moderately differentiated tubular adenocarcinoma	6 (20%)
Poorly differentiated tubular adenocarcinoma	14 (46.7%)
Signet-ring cell carcinoma	4 (13.3%)
Others	4 (13.3%)
Unknown	1 (3.3%)

small animal [18F]FDG PET/MR imaging, and analysis were conducted as previously described [11]. All procedures involving *in-vivo* mouse studies were approved by the Institutional Animal Care and Use Committee (IACUC) at Seoul National University and complied with the Guide for the Care and Use of Laboratory Animals (SNU-170704-3).

Development of a [18F]FDG-avid tumor prediction model (PETscore)

RNA-seq data of 30 GC PDXs paired with animal [18F]FDG-PET data were utilized to develop a model predicting [18F]FDG-avidity. We used Weighted Gene Co-expression Network Analysis (*WGCNA*) package [12] to identify gene network modules from the 30 PET-scanned PDXs (*training set*). The power—the key parameter for the weighted network—was selected to optimize both scale-free topology and sufficient node connectivity and we chose a threshold of 10 in this study. The correlation matrix was transformed into an adjacency matrix (matrix of connection strength) using the power function, and pair-wise topological overlap between genes was calculated. We identified network modules using a hierarchical clustering method with topological overlap dissimilarity as the distance measure. The modules were detected by the dynamic tree cut algorithm, defining a height cutoff value of 0.99, deep split as 4, and minimum module size cutoff value of 40. Genes that were not assigned to any module were classified to color gray (Figure S1).

We selected a gene signature related with SUVmax by the least absolute shrinkage and selection operator (Lasso) regression using *glmnet* R package [13]. The proposed [18F]FDG-avid tumor prediction model using the least absolute shrinkage and selection operator (Lasso) regression can be written as follows:

$$Y'_i = \sum_{j=1}^{p} X_{ij}\beta_j + \beta_0$$

via minimizing $\sum_{i=1}^{n} \left(Y_i - Y'_i\right)^2 + \lambda \sum_{j=1}^{p} \left|\beta_j\right|$,

where Y is actual SUVmax, Y' is predictive SUVmax in PDX, and X is RNA-seq read count for each gene. The n is the total number of PDX cases, p is the total number of genes in the module, and $\lambda \sum_{j=1}^{p} \left|\beta_j\right|$ is the Lasso penalty term. β is the regression coefficient of each variable, which indicates how each gene explains the gene signature. The penalty regularization parameter λ was determined via the cross-validation routine cv.glmnet function (tenfold cross validation). The λ value was finalized by using lambda.1se, which gives the most regularized model such that error is within one standard error of the minimum (Figure S2). For developing of PETscore with the predictive SUVmax, we utilized min–max normalization which results in rescaling the range of SUVmax values to scale the range in [0, 1]. The min–max normalization can be written as follows:

$$x'_i = \frac{x_i - \min\left(x_i\right)}{\max\left(x_i\right) - \min\left(x_i\right)}$$

Here x_i indicates SUVmax of i th samples and x'_i is its PETscore.

This model was assessed using RNA-seq data of 15 patients who underwent FDG-PET in the training set and validated by RNA-seq data and qRT-PCR using GC tissues of patients paired with human [18F]FDG PET data (*validation set*). The overall study flow is summarized in Fig. 1a.

Human tissue specimens for the prediction model validation

PET results and RNA-seq data of 8 GC patients were available for the model validation. Twenty fresh frozen tissues among GC patients who underwent FDG-PET scan were available for additional validation by real-time reverse transcription PCR (qRT-PCR). The clinical characteristics of all patients are shown in Table 2. All tissue samples were obtained from Seoul National University Hospital and written informed consent was obtained from all patients. The present retrospective validation was approved by the IRB of Seoul National University Hospital (No. 1910-045-1069). Each sample was named as follows: 'R_' stands for RNA-seq validation, and 'Q_' stands for qRT-PCR validation.

Statistical analysis

The Spearman's correlation analysis was performed between the predicted SUVmax (PETscore) and the actual SUVmax using *ggplot2* R package [14]. Correlation coefficients and *p*-values were gained and used to sort statistically significant features ($p < 0.05$). A confidence interval of 0.95 was depicted as gray shading. All statistical analyses were performed in R (version 3.5.3).

The linear models for microarray data (*limma*) package [15] was utilized to identify genes associated with SUVmax. False discovery rate (FDR) < 0.05 was used for selecting the genes associated with SUVmax.

Results

Measurement of [18F]FDG uptake in mouse tumor model bearing GC PDXs.

To evaluate FDG avidity in different PDX cases, [18F]FDG-PET imaging was performed for 30 PDX cases using a small-animal PET/MR scanner. Among 30 PDX cases, 15
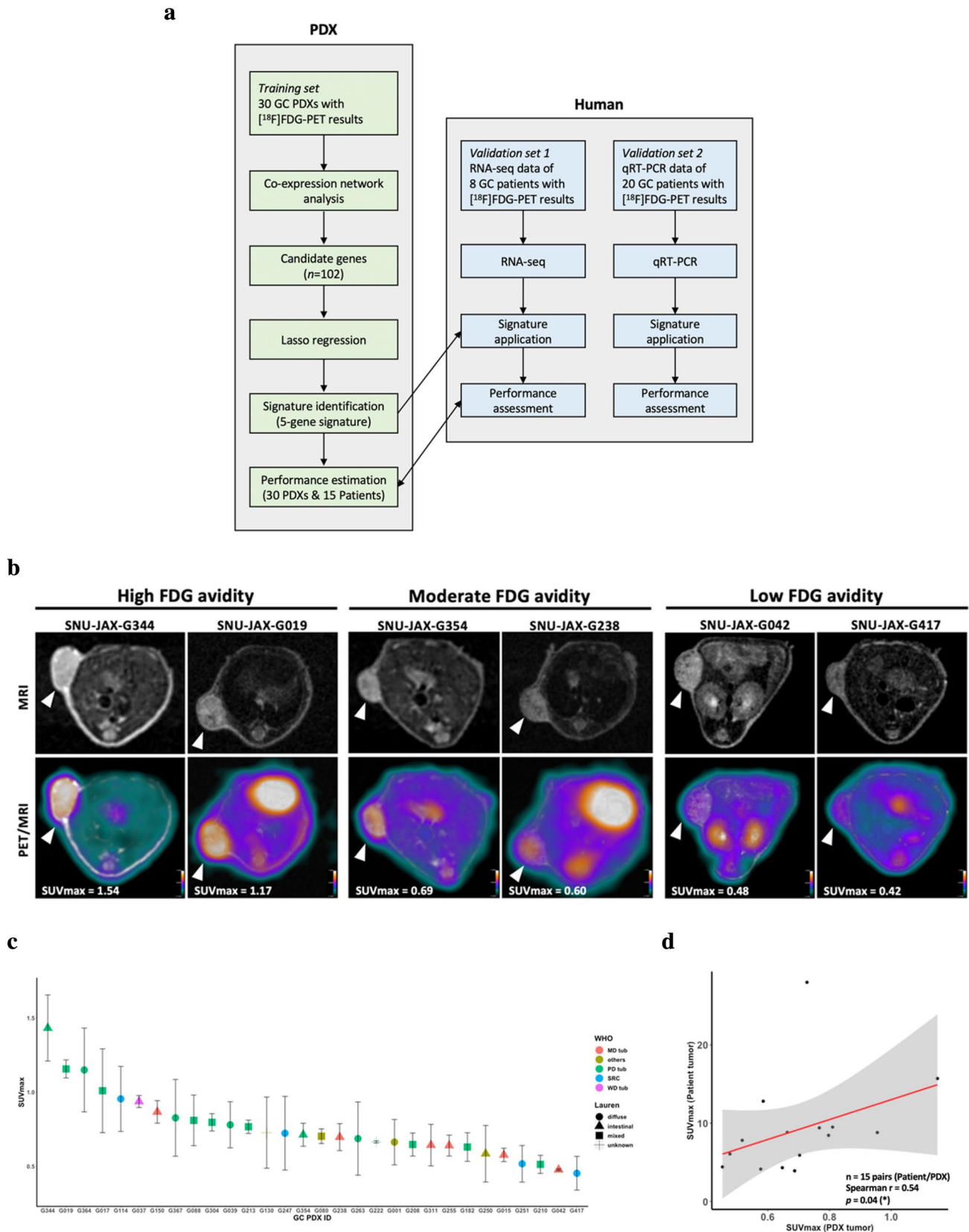
Fig. 1 [18F]FDG uptake in mouse tumor model bearing gastric cancer PDX tissues. **a** Study design. **b** Representative [18F]FDG-PET/MRI images. **c** Quantitative analysis of PET images of PDX tumors. **d** Correlation between parental tumors and corresponding PDXs

Table 2 Characteristics of the PET-scanned advanced gastric cancer patients

Variable	RNA-seq validation	qRT-PCR validation
Total no. of patients	$n = 8$	$n = 20$
Sex		
Male	6	16
Female	2	4
Age, years		
Median (range)	60.5 (46–78)	70 (31–88)
SUVmax		
Median (range)	12.5 (3.91–19.2)	9.6 (3.7–27.3)
TNM stage		
IIa	–	4
IIb	–	2
IIIa	–	2
IIIb	1	7
IIIc	5	1
IV	2	4
Borrmann type[a]		
I	1	3
II	–	4
III	7	8
IV	–	3
Unknown	–	1
Lauren classification[a]		
Intestinal	4	10
Diffuse	3	8
Mixed	–	1
Unknown	1	–

[a]One patient is palliative gastro-jejunostomy bypass case in qRT-PCR validation group

cases had the baseline [18F]FDG-PET images of the parental tumors to compare the [18F]FDG avidity of the parental tumors and PDXs. Overall characteristics of GC PDXs are summarized in Table 1. The median value of the SUVmax of the PDX cases was 0.708 (range 0.453–1.433). Representative images and FDG uptake measurement in tumors of each PDX case are shown in Fig. 1b and c. The SUVmax of PDX tumors were significantly correlated with those of their parental tumors ($n = 15$, Spearman $r = 0.54$, $p = 0.04$) (Fig. 1d). The FDG avidity of each PDX case was used to develop the prediction model.

A gene network module associated with [18F]FDG uptake

We performed a WGCNA on the transcriptome data of PDX tumors. The gene co-expression network was constructed using preprocessed 16,927 genes of PDX. The connectivity between genes in the gene network met a scale-free network distribution with a soft threshold power of $\beta = 10$ (scale-free $R2 = 0.90$) (Figure S1a). After merging similar clusters, 19 co-expression network modules that contained groups of genes with similar patterns of connection strengths with other genes were identified (Figure S1b). The highest association was found between the midnightblue module and SUVmax ($r = -0.92$, $p = 1.8e$-42) (Figure S1c and S1d). This module containing 102 eigengenes was associated with SUVmax and had the highest significance across all modules.

To obtain a primary understanding of the molecular and biological relevance of the midnightblue module, GO enrichment analysis on the 102 genes was performed. From DAVID database, top five enrichment terms were acquired (Fig. 2a). This module was associated with cellular membranes as well as cell–cell communications which control basic cellular activities [16]. In terms of the molecular function and cellular components, the module associated with [18F]FDG uptake included 'cell adhesion molecule binding' and 'cell–cell junction', which are potentially related to diffuse type of GC [17].

PETscore as a [18F]FDG avidity prediction model

Based on the result of WGCNA, the LASSO regression combined with tenfold cross validation was used to create a predictor for SUVmax in the 30 PDX cases (Figure S2). Accordingly, we chose five genes (*PLS1, SLC6A5, NAT16, HBQ1, PYY*) predicting SUVmax in the 30 PDX training set. A gene signature (PETscore) was derived to calculate SUVmax for each PET-scanned PDX based on the expression level of five genes. The predicted SUVmax showed a significantly positive correlation with actual SUVmax (Spearman $r = 0.679$, $p < 1 \times 10^{-4}$) (Fig. 2b). For estimation of the model performance in patients FDG PET, the PETscore was applied to 15 PET-scanned patients who were paired with the 15 PDXs in the training set. The SUVmax of these 15 patients was significantly correlated with the PETscore estimated by RNA-seq of the parental tumor (Spearman $r = 0.557$, $p = 0.034$) (Fig. 2c).

To validate the model in an independent cohort, we applied the model to twenty-eight PET-scanned patients (Table 2 and Fig. 3a). Eight patients among the patients were available to use RNA-seq data. Twenty patients were assessed with the expression of the five genes (*PYY, SLC6A5, HBQ1, PLS1, NAT16*) by qRT-PCR method. The prediction performed with RNA-seq data showed significant correlation with actual SUVmax (Spearman $r = 0.905$, $p = 0.005$) (Fig. 3b). The PETscore measured by qRT-PCR showed a significant positive correlation (Spearman $r = 0.464$, $p = 0.039$) with SUVmax in the 20 patients (Fig. 3c).
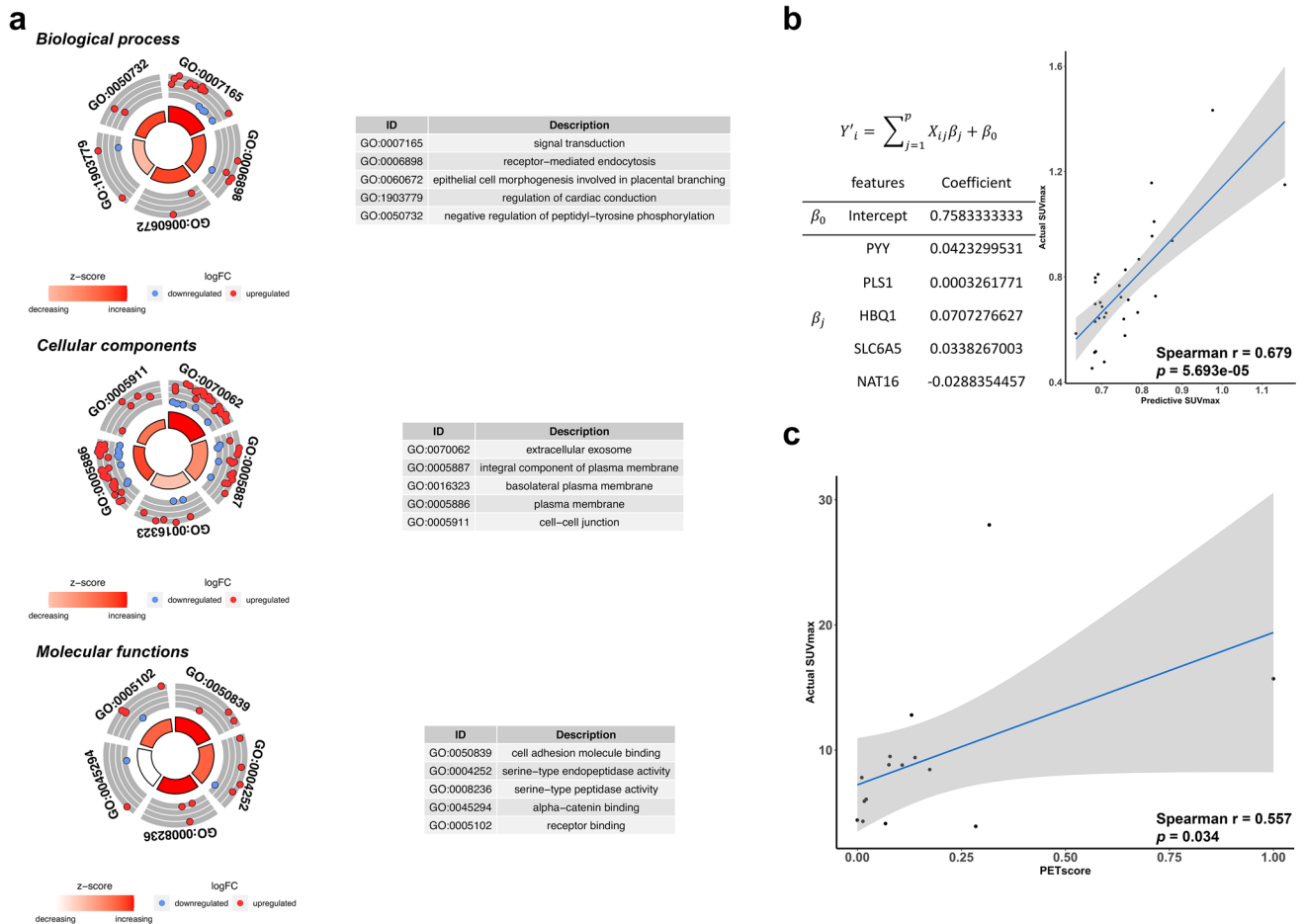
Fig. 2 Establishment of FDG avidity prediction model for gastric cancer. **a** GO analysis of the midnightblue module. **b** A prediction model based on expression levels of the five genes. The formula provided significantly positive correlation between actual SUVmax and predicted SUVmax in PDXs (Spearman $r = 0.679$, $p = 5.693$e-05). **c** PETscore calculated based on the formula in 15 PET-scanned patients showed a positive correlation with actual SUVmax (Spearman $r = 0.557$, $p = 0.034$)

Genomic features associated with PETscore

To investigate the molecular characteristics in gastric cancer being associated with PETscore, it was applied to The Cancer Genome Atlas (TCGA) data. RNA-seq data of TCGA were used to estimate the PETscore of each GC subject. First, we compared PETscore with metabolic features of GC. The metabolic profiles of GC were estimated by single-sample gene set enrichment analysis [18]. The comprehensive relationship between metabolic landscape and PETscore is represented in Fig. 4. Most metabolic profiles showed a trend of positive correlation with PETscore (Figure S3). Gluconeogenesis was a molecular profile with the highest positive correlation with PETscore ($r = 0.2793$, $p = 7.13$E-09). However, glycogenolysis showed the lowest correlation with PETscore ($r = -0.1390$, $p = 0.0045$). Among metabolic features, GLUTs and glycolysis enrichment scores are closely associated with FDG uptake in terms of the mechanism, we tested whether these two features were positively correlated

with PETscore. The PETscore was positively correlated with GLUTs and glycolysis signatures ($r = 0.26$, $p < 0.0001$ for GLUT; Fig. 5a, $r = 0.26$, $p < 0.0001$ for glycolysis; Fig. 5b). In addition, as FDG uptake is lower in diffuse type GC in terms of microscopic morphological classification [9], PETscore according to the morphological types was compared. We confirmed that patients with stomach adenocarcinoma or tubular stomach adenocarcinoma had significantly higher PETscores than diffuse type gastric cancer patients ($p = 0.0206$ for stomach type, $p = 0.0077$ for tubular type; Figure S4).

PETscore tended to be associated with microsatellite instability (MSI) status. The PETscore of GC with MSI-high (MSI-H) was significantly higher than those of MSI-low (MSI-L) and MSS tumors (Fig. 5c). As MSI status affects tumor mutational burden (TMB), the correlation analysis between TMB and PETscore was performed. Accordingly, PETscore showed a significant positive correlation with TMB ($r = 0.29$, $p = 2.1 \times 10^{-8}$) (Fig. 5d).
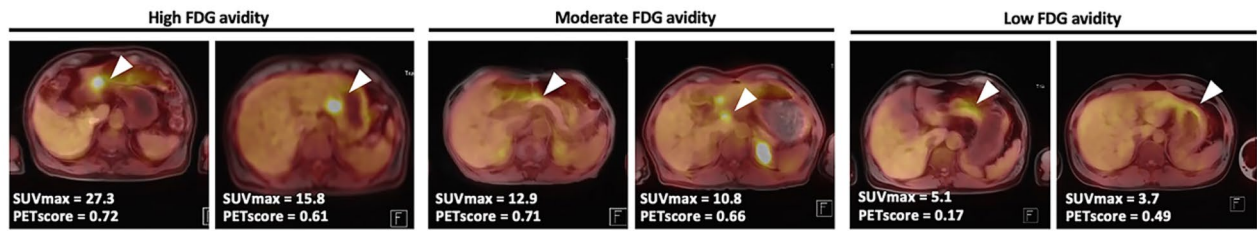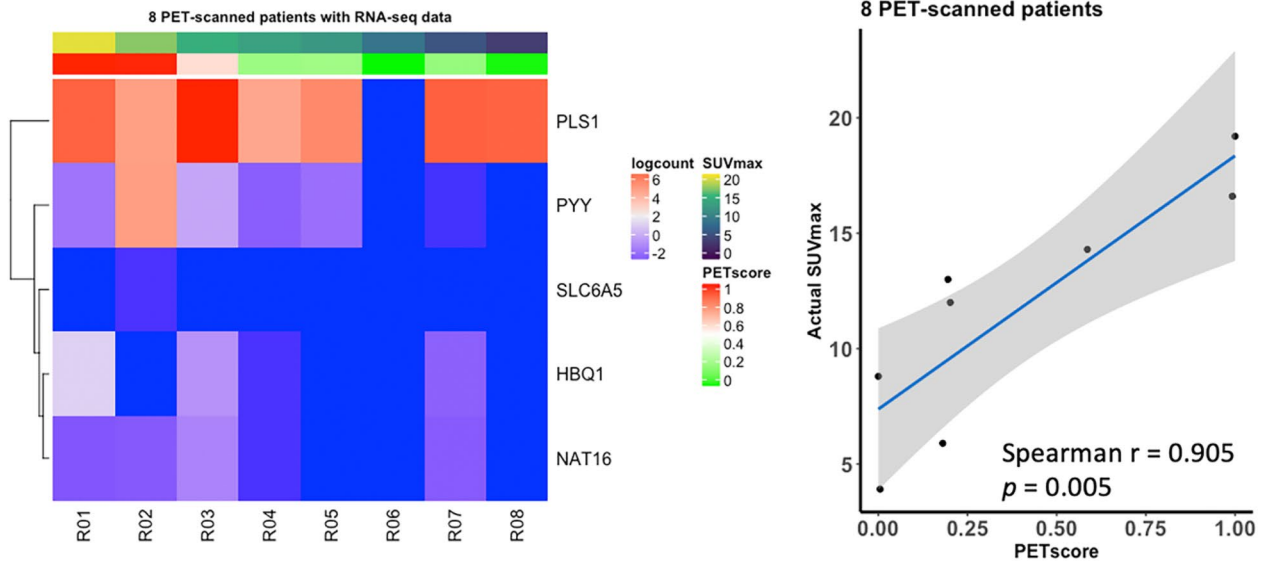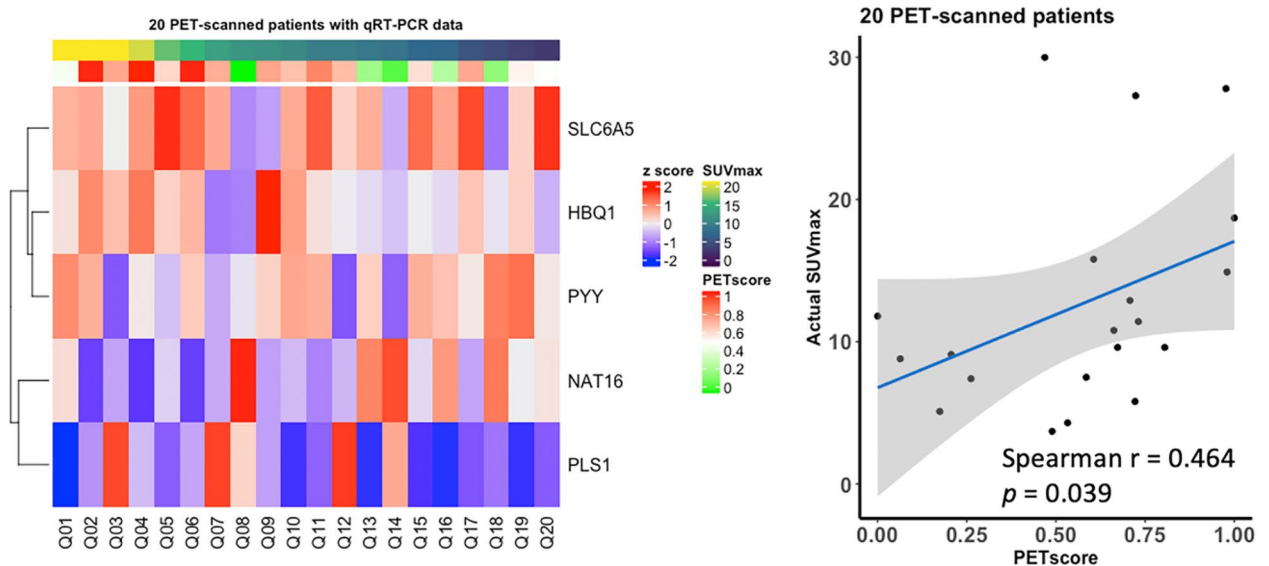
Fig. 3 Validation of the prediction model in human. **a** Representative [¹⁸F]FDG-PET/MRI images of 28 PET-scanned gastric cancer patients. **b** Heatmap displaying the z-scores of the expression levels on the five genes measured by RNA-seq. **c** Heatmap displaying the z-scores of the expression levels on the five genes measured by qRT-PCR. Correlation between SUVmax and results by each validation method showed significantly positive (RNA-seq: Spearman $r = 0.905$, $p = 0.005$, qRT-PCR: Spearman $r = 0.464$, $p = 0.039$)
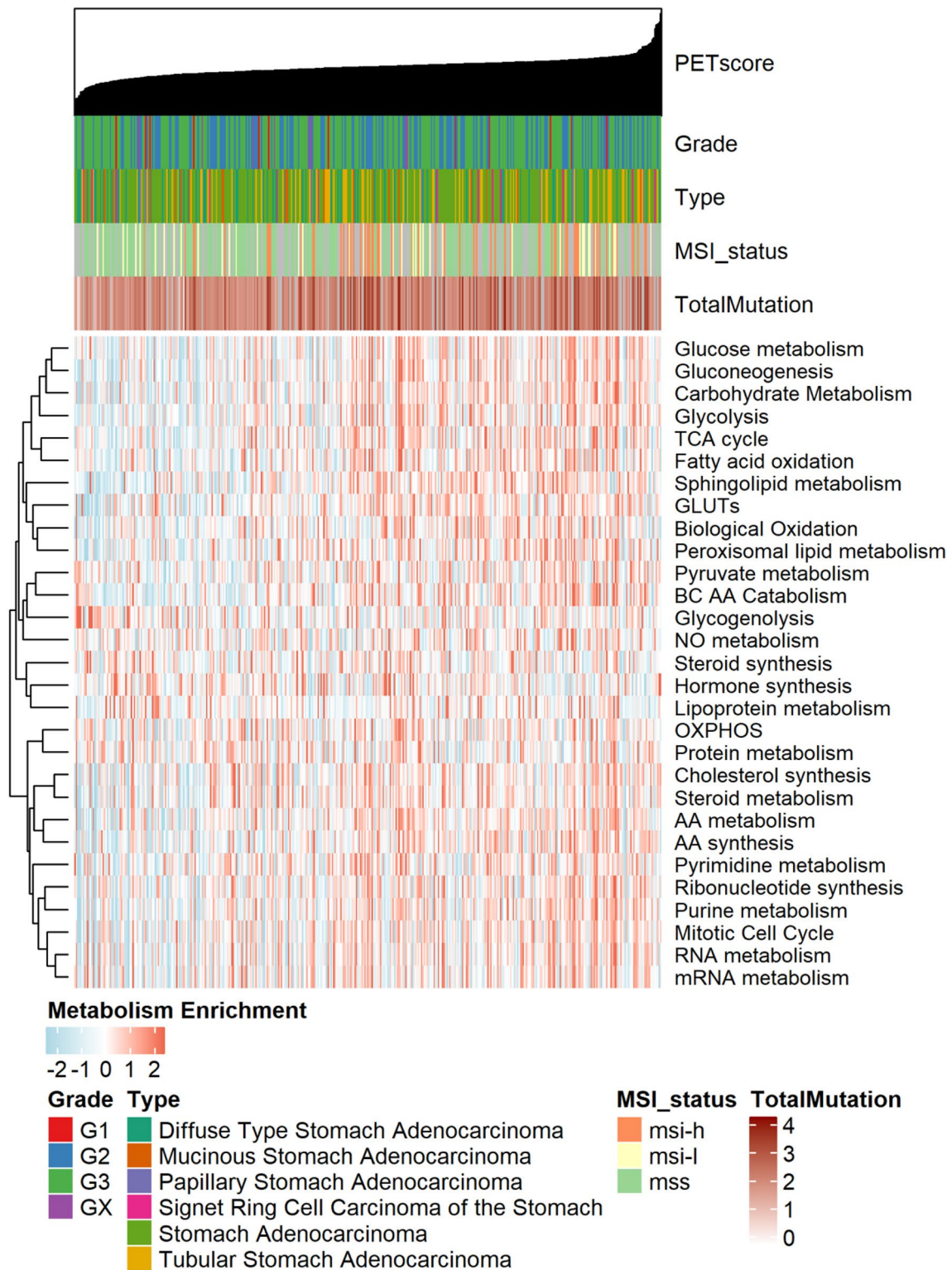
Fig. 4 The comprehensive illustration showing the relationship between molecular characteristic landscape and PETscore. A heatmap depicting the metabolism enrichment scores of all samples. Grade, type by WHO classifications, MSI status, and total mutation are shown for each sample (above the heatmap)

Fig. 5 Molecular characteristic landscape of gastric cancer with PETscore. **a** Scatter plot of PETscore versus GLUTs signature. **b** Scatter plot of PETscore versus glycolysis signature. Both GLUTs and glycolysis signatures was positively correlated with PETsore by Pearson's correlation ($R = 0.26$, $p < 0.0001$). **c** The PETscore was significantly clustered between the MSI status. **d** Colored dots indicate MSI status of each sample, and it shows a trend that samples with high mutation burden are located within populations with high PETscore
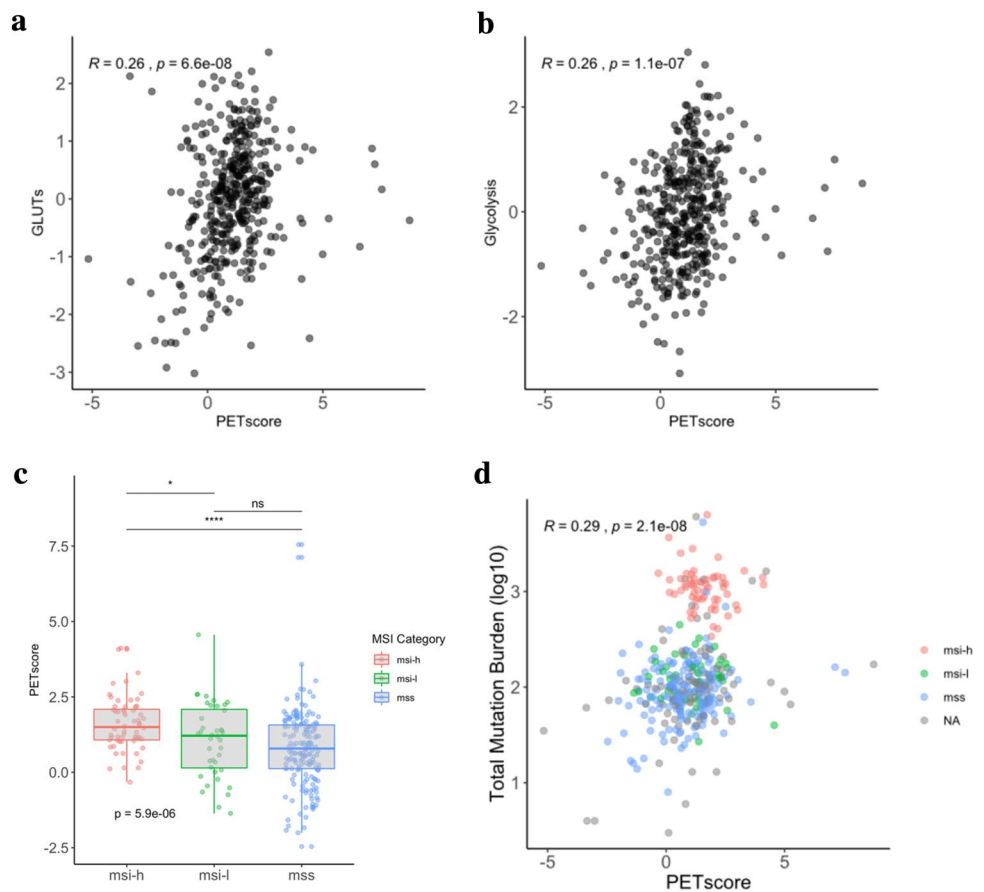
We identified genomic alterations associated with PETscore. Using the median value of PETscore, GC of TCGA were divided into two groups: tumors with high PETscore and low PETscore. Four genes (PLXNA3, EIF4G1, TRIO and PCNX) were identified as differentially mutated genes between PETscore high and low groups (Figure S5). These four genes were more common in GC tumors with high PETscore.

Discussion

[18F]FDG-PET is usually included in staging, response evaluation, and assessment of recurrence as it is an imaging method that noninvasively characterizes tumor metabolism related to biological aggressiveness of the tumor [19]. Because of the diversity of GC, heterogeneous FDG uptake in GC causes a limitation in the clinical application. To understand the metabolic tumor biology of GC affecting variable FDG uptake, we exploratively sought to find functional gene modules potentially being associated with FDG uptake and developed a gene signature to predict FDG avidity in GC. In addition, the association of genomic alterations and the gene signature-based PETscore were investigated to explain the variability of tumor metabolism of GC in terms of molecular features.

Tumor glucose metabolism on a gross-scale represented as FDG uptake is affected by multiple biological features of tumors such as cellularity, hypoxia, vasculature as well as cellular glucose metabolism [20]. Glycolysis is a vital metabolic pathway regulating oncogenes, tumor suppressor genes, and glycolytic enzymes as well as accelerating cell proliferation in malignancies [21]. Glycolytic gene expression is known to be correlated with FDG uptake features. In spite of the individual transcript-level correlation, how the functional gene networks systematically influence the heterogeneous FDG avidity of GC has not been fully understood. WGCNA, a system biology approach aiming to investigate the relationships between genes and phenotype of samples, can be applied to identify complex biological mechanisms responsible for the target phenotypes. The unsupervised hierarchical clustering method selected by WGCNA avoided potential biases and subjective decisions attributed to the selection of the candidate genes previously reported associated with FDG uptake in GC. We applied WGCNA to analyze PET-scanned human GC PDXs to identify genes associated with the SUVmax. The gene module associated with FDG uptake was related to the specific molecular

function and cellular components including cell adhesion and cell–cell junction. These molecular pathways are related to the diffuse type of GC [17], which is a clinically important GC subtype. In particular, the loss of function related to cell adhesion changes the cancer cell to have high epithelia–mesenchymal transition [17, 22]. Furthermore, it is well known that diffuse type according to Lauren classification and poorly cohesive carcinoma according to WHO classification showed low FDG uptake [23].

We identified a novel gene signature with five genes (Up-regulated: *PLS1, PYY, SLC6A5, HBQ1;* Down-regulated: *NAT16*) associated with high SUVmax in GC. Among the five genes in our PETscore, *PLS1* gene is overexpressed in colorectal cancer [24]. Peptide YY (*PYY*) is a gut hormone and has been identified in several carcinoid tumors including rectal carcinoids [25], gastric, small bowel and cecal endocrine tumors [26, 27]. Solute Carrier Family 6 Member 5 (*SLC6A5*) is known as the glycine transporter gene *GLYT2* and it is associated with medulloblastoma [28], prostate cancer [29], oral and pharyngeal cancer [30]. Borgan et al. reported that hemoglobin subunit theta 1 (*HBQ1*) was differentially expressed in breast cancer after combination of bevacizumab and doxorubicin [31]. N-Acetyltransferase 16 (*NAT16* or *C7orf52*), encodes histidine *N*-acetyltransferase. TCGA thyroid cancer data showed *C7orf52* was one of differentially downregulated genes in papillary thyroid cancer patients with lymph node metastasis [32]. In summary, previous studies regarding these molecules consisting of PETscore associated with prognosis or aggressiveness in GCs are hardly found. Nonetheless, these gene sets may reflect the metabolic profile of GCs, suggesting that they can be novel molecular features related to various biological features of GC. As a future study, the association with GC for each gene of the signature needs to be investigated.

The gene signature for PETscore could be used as an adaptive management strategy of GC. The suggested model could be extended to molecular profiles of GC to be used in the clinical setting to perform an individualized and rational approach for choosing imaging modality. If we could predict biological profiles of GC with high FDG uptake, [^{18}F] FDG-PET in this context can be evaluated as a diagnostic, treatment response and recurrence monitor tool for selected patients. In this clinical setting, the reliability of [^{18}F]FDG-PET precisely used according to the PETscore is expected to be increased significantly. If the primary GC has the characteristics of high FDG uptake, FDG uptake will be high for recurrent or metastatic lesions, so predicting the biology of GC can lead to an individualized approach. Example cases are shown in (Figure S6a and S6b). A tumor that showed the low PETscore was also low FDG avidity in a recurred tumor at 1-year follow-up. On the other hand, another tumor with high PETscore showed hypermetabolism in recurred retroperitoneal LNs and peritoneal seeding lesions. The gene

signature can be assessed by biopsy tissues, PETscore may be used for an individualized approach for imaging modality by predicting FDG-avidity of the tumor (Figure S6c). These findings provide the opportunity to include a rational selection process for GC [^{18}F]FDG-PET clinical evaluation.

GC with microsatellite instabilities high (MSI-H) was proposed as a distinct subgroup of GCs [33, 34]. Choi et al. reported that STAD (Stomach Adenocarcinoma) and COAD (Colon adenocarcinoma) showed a larger number of the metabolism-related genes than other cancer types investigating the relationship between metabolic profiles and MSI status [18]. Notably, our results concordantly showed that MSI-H with a high PETscore had a hypermutation burden (Fig. 5d). MSI-H GCs are more likely to result in favorable survival than low-level MSI (MSI-L) or microsatellite stable (MSS) tumors and associated with both high Tumor-infiltrating lymphocytes (TILs) and programmed death-ligand 1 (PD-L1) [35]. MSI status is considered as a biomarker for therapeutics with immune-checkpoint inhibitors [36, 37]. In this regard, it is notable that the association between MSI status and PETscore can be further investigated to develop a predictive noninvasive bio-imaging marker for the assessment of MSI-status. In the clinical setting, in order to decide MSI status, the results of FDG uptake could be used if FDG non-avid GC can exclude MSI-H even though a further well-designed prospective study is needed.

Certain limitations should be noted for this study. Functional analysis and understanding of the genes being included in PETscore are pending as focus was put on internal and external validation of the score itself. Further investigations are addressing this question as it is necessary for a full understanding of the causal relationship of glucose metabolic pathways with these genes and its practical application in GC. Second, larger and potentially international cohorts have to be used for further validation of the present findings' proofing to also overcome the potential regional heterogeneities of GC. Application on the TCGA cohort can be seen as one important step in this manner.

Non-invasive prediction of FDG avidity is critical for developing better therapeutic strategies in terms of care and elucidating the underlying metabolic underpinnings of heterogeneous GC. This study identified a gene module associated with [^{18}F]FDG uptake. The module represented 'cell adhesion molecule binding' and 'cell–cell junction'. Using gene sets in this module, we developed a five-gene signature for FDG avidity prediction in GC, PETscore. Association of the PETscore and MSI status was found by applying it to a multi-omics database (TCGA). As a novel aspect, this study analyzes the variable glucose metabolism in GC by integrating metabolic imaging in transcriptome and genomic data. These findings suggest that molecular characteristics are underlying the diverse metabolic profiles of GC, eventually leading to personalized diagnostic and therapeutic pathways.

Data availability Data that support this study can be made available upon reasonable request.

Declarations

Conflict of interest The authors declare that they have no conflict of interest.

Ethical approval All institutional and national guidelines for the care and use of laboratory animals were followed.

References

1. Gullo I, et al. Heterogeneity in gastric cancer: from pure morphology to molecular classifications. Pathobiology. 2018;85(1–2):50–63.
2. Vergadis C, Schizas D. Is accurate N—staging for gastric cancer possible? Front Surg. 2018;5:41.
3. Bomanji JB, Costa DC, Ell PJ. Clinical role of positron emission tomography in oncology. Lancet Oncol. 2001;2(3):157–64.
4. Hirayama A, et al. Quantitative metabolome profiling of colon and stomach cancer microenvironment by capillary electrophoresis time-of-flight mass spectrometry. Cancer Res. 2009;69(11):4918–25.
5. Yun M, et al. Lymph node staging of gastric cancer using (18)F-FDG PET: a comparison study with CT. J Nucl Med. 2005;46(10):1582–8.
6. Kim SK, et al. Assessment of lymph node metastases using 18F-FDG PET in patients with advanced gastric cancer. Eur J Nucl Med Mol Imaging. 2006;33(2):148–55.
7. Lordick F, et al. PET to assess early metabolic response and to guide treatment of adenocarcinoma of the oesophagogastric junction: the MUNICON phase II trial. Lancet Oncol. 2007;8(9):797–805.
8. De Potter T, et al. Whole-body PET with FDG for the diagnosis of recurrent gastric cancer. Eur J Nucl Med Mol Imaging. 2002;29(4):525–9.
9. Stahl A, et al. FDG PET imaging of locally advanced gastric carcinomas: correlation with endoscopic and histopathological findings. Eur J Nucl Med Mol Imaging. 2003;30(2):288–95.
10. Mochiki E, et al. Evaluation of 18F-2-deoxy-2-fluoro-D-glucose positron emission tomography for gastric cancer. World J Surg. 2004;28(3):247–53.
11. Bae S-W, et al. Establishment of a [18F]-FDG-PET/MRI imaging protocol for gastric cancer PDX as a preclinical research tool. J Gastric Cancer. 2020;20(1):60–71.
12. Langfelder P, Horvath S. WGCNA: an R package for weighted correlation network analysis. BMC Bioinformatics. 2008;9:559.
13. Friedman J, Hastie T, Tibshirani R. Regularization paths for generalized linear models via coordinate descent. J Stat Softw. 2010;33(1):1–22.
14. Wickham H. Ggplot2: elegant graphics for data analysis. In: Use R!, vol. viii. New York: Springer; 2009. p. 212.
15. Ritchie ME, et al. Limma powers differential expression analyses for RNA-sequencing and microarray studies. Nucleic Acids Res. 2015;43(7):e47.
16. Bradshaw RA, Dennis EA. Handbook of cell signaling. Amsterdam San Diego, Calif: Academic Press; 2004.
17. Ge S, et al. Author correction: a proteomic landscape of diffuse-type gastric cancer. Nat Commun. 2018;9(1):1850.
18. Choi H, Na KJ. Pan-cancer analysis of tumor metabolic landscape associated with genomic alterations. Mol Cancer. 2018;17(1):150.
19. Brenkman HJF, et al. Evaluation of PET and laparoscopy in STagIng advanced gastric cancer: a multicenter prospective study (PLASTIC-study). BMC Cancer. 2018;18(1):450.
20. Mochizuki T, et al. FDG uptake and glucose transporter subtype expressions in experimental tumor and inflammation models. J Nucl Med. 2001;42(10):1551–5.
21. Cairns RA, Harris IS, Mak TW. Regulation of cancer cell metabolism. Nat Rev Cancer. 2011;11(2):85–95.
22. Huang L, Wu RL, Xu AM. Epithelial-mesenchymal transition in gastric cancer. Am J Transl Res. 2015;7(11):2141–58.
23. Kim HW, et al. Correlation of primary tumor FDG uptake with histopathologic features of advanced gastric cancer. Nucl Med Mol Imaging. 2015;49(2):135–42.
24. Zhang T, et al. Plastin 1 drives metastasis of colorectal cancer through the IQGAP1/Rac1/ERK pathway. Cancer Sci. 2020;111(8):2861–71.
25. Fiocca R, et al. Glucagon, glicentin, proglucagon, PYY, PP and proPP-icosapeptide immunoreactivities of rectal carcinoid tumors and related non-tumor cells. Regul Pept. 1987;17(1):9–29.
26. Iwafuchi M, et al. Peptide YY immunoreactive cells in gastrointestinal carcinoids: immunohistochemical and ultrastructural studies of 60 tumors. Hum Pathol. 1986;17(3):291–6.
27. Hayashi H, et al. Immunohistochemical analysis of gastrointestinal carcinoids. Gastroenterol Jpn. 1993;28(4):483–90.
28. Margol AS, et al. Tumor-associated macrophages in SHH subgroup of medulloblastomas. Clin Cancer Res. 2015;21(6):1457–65.
29. Bert SA, et al. Regional activation of the cancer genome by long-range epigenetic remodeling. Cancer Cell. 2013;23(1):9–22.
30. Langevin SM, et al. CpG island methylation profile in non-invasive oral rinse samples is predictive of oral and pharyngeal carcinoma. Clin Epigenetics. 2015;7:125.
31. Borgan E, et al. Subtype-specific response to bevacizumab is reflected in the metabolome and transcriptome of breast cancer xenografts. Mol Oncol. 2013;7(1):130–42.

32. Xin YL, et al. The TGF-beta-regulated X-inactive tran-script inhibits papillary thyroid cancer migration and invasion. Transl Cancer Res. 2018;7(4):958.

33. Cancer Genome Atlas Research, N. Comprehensive molec-ular characterization of gastric adenocarcinoma. Nature. 2014;513(7517):202–9.

34. Cristescu R, et al. Molecular analysis of gastric cancer identifies subtypes associated with distinct clinical outcomes. Nat Med. 2015;21(5):449–56.

35. Kim ST, et al. Comprehensive molecular characterization of clini-cal responses to PD-1 inhibition in metastatic gastric cancer. Nat Med. 2018;24(9):1449–58.

36. Fuchs CS, et al. Safety and efficacy of pembrolizumab mono-therapy in patients with previously treated advanced gastric and gastroesophageal junction cancer: phase 2 clinical keynote-059 Trial. JAMA Oncol. 2018;4(5):180013.

37. Ratti M, et al. Microsatellite instability in gastric cancer: molecu-lar bases, clinical perspectives, and new treatment approaches. Cell Mol Life Sci. 2018;75(22):4151–62.